

Interaction of YD2 and TiO₂ in dye-sensitized solar cells (DSSCs): a density functional theory study

Fernando Mendizabal^{1,5} · Alfredo Lopéz^{1,2} · Ramiro Arratia-Pérez^{3,5} · Natalia Inostroza⁴ · Cristian Linares-Flores⁴

Received: 6 May 2015 / Accepted: 20 July 2015 / Published online: 13 August 2015
© Springer-Verlag Berlin Heidelberg 2015

Abstract The interaction of the dye YD2 with a cluster of (anatase-phase) TiO₂ (which is utilized in dye-sensitized solar cells, DSSCs) and electron injection by the dye into the cluster were studied by performing density functional theory (DFT) calculations at the B3LYP, PBE, and TPSS levels of theory, including dispersion effects. We studied and quantified the interaction of the metallomacrocyclic with the TiO₂ cluster and the electronic spectrum of the complex. TDDFT calculations using the B3LYP functional were found to be the most suitable for describing the observed absorption energy bands of YD2 and YD2–TiO₂. Our calculations show that the diarylamino groups act as electron donors in the photon-induced injection that occurs in DSSCs. The free-energy changes that take place during electron injection support the good performance of YD2 on TiO₂ clusters.

Electronic supplementary material The online version of this article (doi:10.1007/s00894-015-2771-5) contains supplementary material, which is available to authorized users.

✉ Fernando Mendizabal
hagua@uchile.cl

- ¹ Departamento de Química, Facultad de Ciencias, Universidad de Chile, Las Palmeras 3425, P.O. Box 653, Ñuñoa, Santiago, Chile
- ² Departamento de Química, Facultad de Ciencias Básicas, Universidad Metropolitana de Ciencias de la Educación, Casilla 147, Santiago, Chile
- ³ Doctorado en Físicoquímica Molecular, Relativistic Molecular Physics (ReMoPh) Group, Universidad Andrés Bello, República 275, Santiago, Chile
- ⁴ Inorganic Chemistry and Molecular Materials Group, Facultad de Ingeniería, Universidad Autónoma de Chile, El Llano Subercaseaux 2801, San Miguel, Santiago, Chile
- ⁵ Millennium Nucleus “Molecular Engineering for Catalysis and Biosensors”, Santiago, Chile

Keywords YD2–TiO₂ model · Coordination energies · Absorption spectra · TDDFT

Introduction

Supramolecular systems can be designed to have specific functionalities and properties (e.g., light conversion or nonlinear optics, or to act as molecular wires, self-assembling molecular channels, or chemical sensors) [1]. The noncovalent interactions associated with these properties are hydrogen bonding, π – π stacking, charge transfer, metal coordination, and electrostatic, metallophilic, and hydrophobic interactions [2–4]. Within this broad field, we are interested in evaluating the effects of complexes of transition metals such as metalloporphyrins (MPs), since they are important components in supramolecular organization due to their ability to generate potential interactions and direct structural organization [5–7]. These complexes have unique structural properties, leading to novel functions and applications; for instance, they can act as sensitizers when deposited on semiconductor electrodes (for example TiO₂) in solar energy harvesting and conversion devices [8, 9].

Solar energy will be an important sustainable energy source in the future, even though a variety of energy sources will need to be explored until solar energy harvesting and conversion technology is mature enough to replace more established energy sources [10, 11]. Only 0.02 % of the solar radiation incident on the Earth’s surface has to be captured to satisfy future energy needs. Many different principles have been proposed for constructing efficient devices for capturing solar energy. In the last two decades, dye-sensitized solar cells (DSSCs) have attracted much attention, and attempts are now being made to replace commercial solar cells made with silicon [9]—which have high production and maintenance

costs, leading to a continuous search for replacements—with DSSCs. DSSCs were first proposed by Grätzel [8]. The chemical and physical processes of Grätzel cells are widely known, but the details of what happens in these cells at the atomic level are still rather vague.

Grätzel's DSSCs are based on the adsorption of metallic complexes (e.g., ruthenium and zinc), which are usually termed “dyes” in this context, on nanocrystalline titanium dioxide films [9, 12–19]. Among the dye compounds studied, ruthenium(II) bipyridyl complexes have proven to be the most efficient TiO_2 sensitizers [13–17]. The efficiency of a solar cell is measured by its power conversion index (η). Grätzel cells based on the sensitization of TiO_2 by molecular dyes have η values of 7–11 %. This level of efficiency makes applications feasible. However, ruthenium is an expensive metal, so novel dyes are desirable for the development of novel highly efficient DSSCs [9]. Recently, alternative dyes to ruthenium complexes have been reported in the literature. These dyes contain large π – π aromatic molecules such as metalloporphyrins (MPs), and they constitute an important class of sensitizers on TiO_2 [20–26]. The central metal in the dye is zinc. The resulting highly efficient DSSCs have good photostability and light-harvesting capabilities, with η values of about 6–10 %, close to those of DSSCs with dyes based on ruthenium complexes [13]. Among the most efficient of these Zn-based dyes are YD2, YD2-o-C8, ZnPBAT, and LD14 [27, 28].

Our research has focused on solar cells that utilize Zn-porphyrin (ZnP)-based dyes. All of the ZnP-based sensitizers with antenna molecules described above were designed and applied in DSSCs. The resulting systems show metallosupramolecular interactions, enhancing the light-harvesting efficiency of the DSSC. Performance optimization of devices that use push-pull zinc macrocycles leads to high power-conversion efficiency. For example, the YD2 system yields $\eta=11$ %, and has opened up a new field in porphyrin-based DSSC research [21]. The high performance of YD2 is due to the introduction of diarylamino groups at the *meso* position on the porphyrin ring. Different research groups have designed macrocycles containing different functional groups (e.g., phenyl, dodecyl, pyrene) at various positions on the ring. In general, these groups are donor–acceptor (D–A) substituents with promising photovoltaic properties [29–32]. Also, some of the previously studied systems have been structured into a single supramolecular assembly that is able to absorb a large portion of the solar spectrum in the region between the visible and the near-IR. However, it has been mentioned in several studies that supramolecular interactions are only rarely used in solar cells.

One important aspect of DSSCs is the interaction between the dye sensitizer and the TiO_2 . The sensitizer molecules usually have a carboxyl group that interacts with the solid electrode. This is a fundamental influence on the geometric

structure of the adsorbed dye state and the electronic coupling with the $\text{Ti}(3d)$ conduction band. Over the past 5 years, a number of theoretical studies of solar cells utilizing ruthenium complexes that were performed at the quantum chemical (density functional theory) level and the molecular dynamics level have been published [18–20, 33–39]. Those studies modeled the interaction of the ruthenium sensitizer with the (101) plane of (anatase) TiO_2 or a nanocluster of TiO_2 . The theoretical results obtained indicated that the dye is attached via carboxylate groups.

The aim of the work reported in the present paper was to extend this idea to supramolecular systems, using the well-known coordination preference of the dye YD2. We used YD2 instead of other dyes such as YD2-o-C8, ZnPBAT, and LD14 because the molecular structure of YD2 forms the basis for other, more complex, dyes. The design of supramolecular interactions in solar cells is currently inadequate. It is worth noting that there are natural supramolecular antenna complexes which harvest light. A better understanding of the chemical bonding between the TiO_2 surface and the dye is required. Thus, we performed a theoretical study to find out which anchor groups improve the conjugation with the macrocycle rings. The model systems considered in the calculations consisted of a dye attached to a TiO_2 cluster representing the TiO_2 surface [34–39]. Theoretical models including optimized molecular structures were used to identify and characterize suitable light-capturing molecules. Ground-state calculations showed how the dye binds to TiO_2 . Single-point quantum-chemical calculations of the excited states provided excitation energies and information about the vertical excitation processes. The light-absorption process in dye-sensitized solar cells was studied using time-dependent density functional theory (TDDFT). Determining the nature of the interaction between YD2 and TiO_2 should lead to a better understanding of the rest of the mechanism that occurs in these solar cells and aid the design of new and improved systems.

Models and computational details

The YD2 model used in this study is depicted in Fig. 1. C_1 symmetry was adopted for the dye. The geometry of YD2 in the ground state was fully optimized at the scalar quasi-relativistic B3LYP, PBE, and TPSS levels in the gas and solvent (acetonitrile) phases. Moreover, we were interested in studying the formation of supramolecular systems, where weak and coordination interactions are important. Grimme's dispersion correction was used for those functionals for which they are available, and its use is indicated below by appending “DFT-D3” to the acronym of the density functional [40, 41].

The fully relaxed structure of the dye YD2 adsorbed on the TiO_2 surface was obtained (see Fig. 2). The structure of TiO_2 was kept fixed. We used two approaches for the YD2– TiO_2 interaction model (C_1 symmetry). The first considered a dye

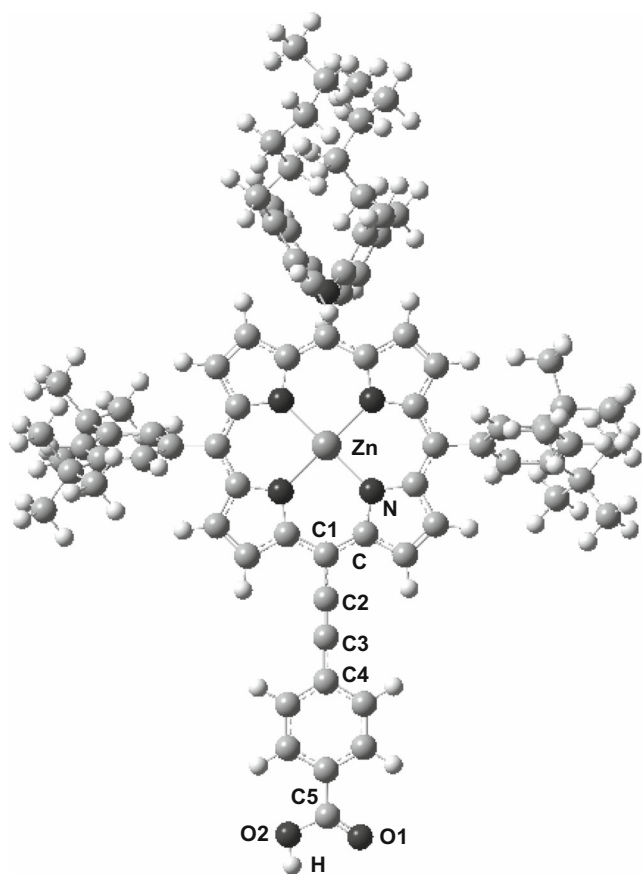
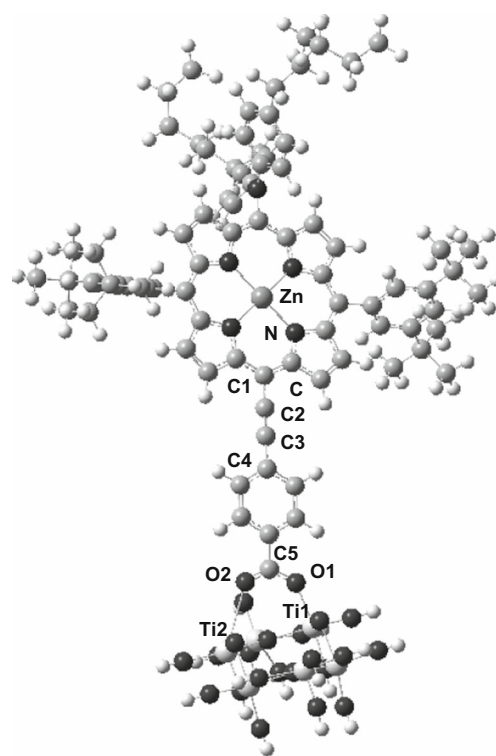


Fig. 1 YD2 dye sensitizer model

molecule without a proton in the $-\text{COOH}$ group; this effect is consistent with the results of experimental and theoretical studies of different porphyrins where carboxylic acid is bound to the TiO_2 surface by means of mono- and bidentate bridging modes. Depending on the dye, mono- or bidentate coordination is observed [42–45]. With respect to the $-\text{COO}^-$ group, it is well known that the experimental IR spectrum exhibits a significant increase in the symmetric carboxylate band at around 1400 cm^{-1} [28]. The disappearance of this $\text{C}=\text{O}$ frequency confirms that a proton detaches from the carboxylic acid group during porphyrin adsorption on TiO_2 . This situation was studied and theoretical models were tested. The second approach utilized a TiO_2 surface model. In the literature there are many such models of various shapes and sizes, ranging from Ti_5 to Ti_{80} [14, 15]. Small-scale theoretical models of TiO_2 have been used to study the interactions of different dyes (N749, N3, C101, J3, etc.) and were found to give reasonable results [46, 47]. In the present work, a $[\text{Ti}_6\text{O}_{21}\text{H}_{18}]$ model was cut from the crystal structure of anatase and employed to simulate the surface of TiO_2 . H atoms were used to saturate the covalent bonds of the O atoms.

The excitation energies were obtained at the DFT level by means of the time-dependent perturbation theory approach (TD-DFT) [48–50]. The excitation spectrum was simulated from the optimized geometry of the theoretical model. The



YD2- TiO_2 Anatase (101)

Fig. 2 YD2 on TiO_2 model

spin-orbit coupling was not evaluated in the TD-DFT calculations, and the values were averaged. All UV/Vis spectra showed Gaussian curves with a full width at half-maximum (FWHM) of 1500 cm^{-1} . Moreover, we used the AOFORCE module [51] implemented in Turbomole [52] to estimate the vibrational frequency of the $-\text{COOH}$ group in free YD2 and in YD2 attached to TiO_2 via $-\text{COO}^-$.

The polarizable continuum model (PCM) was applied to simulate the effects of the solvent (acetonitrile), using the Cosmos program [53]. In addition, the counterpoise correction for basis-set superposition error (BSSE) was used for the calculated interaction energies between YD2 and TiO_2 .

The calculations were performed using the Turbomole package (version 6.5) [52]. For Zn and Ti, the 10-valence-electron (VE) quasi-relativistic (QR) pseudopotential (PP) of Andrae et al. [54] was employed. We used two d -type polarization functions on Zn and Ti [55]. C, N, and O were treated with PPs, using double-zeta basis sets with the addition of one d -type polarization function [56]. For the H atom, a double-zeta basis set plus one p -type polarization function was used [57]. The basis sets were taken as $(6s5p3d|8s7p6d)$ for Zn, $(6s5p3d|8s7p6d)$ for Ti, $(2s-2p1d|4s4p1d)$ for O, $(2s2p1d|4s4p1d)$ for C, $(2s2p1d|4s4p1d)$ for N, and $(2s1p|4s1p)$ for H. All geometry calculations were performed using the efficient resolution of identity (RI) approximation [58].

Table 1 Main geometric parameters (bond lengths and angles) of the YD2 ligand calculated at different levels of theory, including gas and solvent effects (“solv”)

Method	Zn–N (pm)	N–C (pm)	C–C1 (pm)	ZnNCC1 (°)	C2–C3 (pm)	NCC1C2 (°)	C5–O1 (pm)	C5–O2 (pm)	O2C5O1 (°)
B3LYP	204.7	137.8	140.9	2.7	121.7	178.5	123.4	138.3	121.1
TPSS	205.1	138.6	141.7	2.9	122.8	178.8	124.5	139.7	121.1
PBE	205.1	138.4	141.2	2.9	122.9	178.8	124.4	139.3	121.3
B3LYP-D3	204.3	137.6	140.6	2.7	121.5	178.2	123.2	138.1	121.0
TPSS-D3	204.9	138.4	141.6	2.8	122.5	178.9	124.1	139.3	121.0
PBE-D3	204.9	138.2	141.1	2.8	122.5	178.9	123.9	139.3	121.1
B3LYP (solv)	205.1	137.9	141.1	3.1	121.8	178.6	124.0	137.2	121.3
TPSS (solv)	205.2	138.3	141.2	2.9	122.7	178.5	124.7	139.6	121.3
PBE (solv)	205.5	138.4	141.8	3.1	123.8	178.7	124.9	138.1	121.6
B3LYP-D3 (solv)	204.9	137.5	141.0	2.5	121.6	178.5	123.8	137.1	120.5
TPSS-D3 (solv)	205.0	138.1	141.1	2.8	122.1	178.2	124.5	139.3	121.1
PBE-D3 (solv)	205.2	138.3	141.5	2.9	123.4	178.3	124.5	137.8	121.2

Results and discussion

Geometric structures and YD2–TiO₂ coordination energy

The optimized geometry of YD2 calculated at each level of theory is shown in Fig. 1. YD2 is composed of various functional groups: a diarylamino group with two hexyl chains attached to the porphyrin ring acting as electron donor, the phenylethynyl group that forms part of the bridge, the carboxylic acid moiety that acts as an acceptor, and the porphyrin chromophore, which is the π -bridge in this particular donor–(π -conjugated bridge)–acceptor (D– π -A) structure. The selected geometric parameters are listed in Table 1. The bond lengths, bond angles, and dihedrals are very similar whichever level theory is used and regardless of the phase (gas or solvent) considered. The inclusion of dispersion at the D3 level does not

produce major changes. These results are in agreement with other published calculations [59].

We linked YD2 with the TiO₂ model (see Fig. 2) through the carboxylate and the Ti atoms in the (101) plane. The YD2 was fully optimized in its ground state, and the main parameters are shown in Table 2. It can be seen that the structural parameters change upon shifting from free YD2 to YD2–TiO₂. The most relevant changes in the geometry of YD2 when it is coordinated with TiO₂ are seen in the angles ZnNCC2 and NCC1C2, which show a small loss of planarity. The most relevant changes in geometry focus on the carboxylate group, which acts as a monodentate ligand with TiO₂. According to the calculations, the O1 and Ti1 bond lengths are between 199.8 pm and 202.3 pm depending on the method and the medium considered. In general, there is only minor variation in this Ti–O distance. The second distance, Ti2–O2, is longer (between 306.6 pm and 297.7 pm) and retains a

Table 2 Main geometric parameters (bond lengths and angles) of YD2–[TiO₂], as calculated at different levels of theory, including gas and solvent effects (“solv”)

Method	Zn–N (pm)	N–C (pm)	ZnNCC2 (°)	NCC1C2 (°)	Ti1–O1 (pm)	Ti2–O2 (pm)	C5–O2 (pm)	C5–O1 (pm)	O2C5O1 (°)
B3LYP	204.7	136.5	4.5°	174.9°	200.2	304.4	122.9	129.5	128.7°
TPSS	205.1	137.2	3.6°	175.4°	199.8	297.7	123.9	130.4	128.9°
PBE	205.2	136.9	3.9°	175.5°	201.2	300.7	123.9	130.0	129.0°
B3LYP-D3	204.7	136.5	4.4°	174.9°	199.3	299.0	122.9	129.5	128.9°
TPSS-D3	205.1	137.2	4.4°	175.1°	199.5	293.7	124.1	130.4	129.1°
PBE-D3	205.2	136.9	4.6°	174.9°	200.7	295.6	123.9	130.0	129.2°
B3LYP (solv)	204.9	136.3	4.5°	174.8°	201.0	307.4	123.5	129.7	127.2°
TPSS (solv)	205.2	137.0	3.3°	175.3°	200.3	298.6	124.2	130.7	128.3°
PBE (solv)	205.5	136.8	4.1°	174.9°	202.3	306.6	124.5	130.2	127.4
B3LYP-D3 (solv)	204.5	136.1	4.8°	175.1°	200.6	299.5	123.4	129.5	127.8°
TPSS-D3 (solv)	205.1	136.9	3.1°	175.0°	199.8	295.6	124.0	130.3	128.8°
PBE-D3 (solv)	205.5	136.8	4.7°	174.4°	201.6	299.8	124.6	130.1	127.7

slightly bidentate character. The Ti–O distances are slightly shorter when the dispersion effect (D3) and the solvent medium are included in the calculations. The distances C5–O2 and C5–O1 and the angle O2C5O1 when YD2 is bound result in a more relaxed geometry than when YD2 is free.

We estimated the vibrational frequencies of the YD2 dye when it is free and when it is coordinated to the TiO₂ cluster. These results were obtained at the B3LYP-D3 level in the gas phase. In particular, we focused on the vibrational frequency of the –COO[−] group. For the free dye, a vibrational frequency of 1665 cm^{−1} is obtained, which is close to the reported experimental value of 1700 cm^{−1} [28]. On the other hand, when YD2 is linked with TiO₂, the vibrational frequency decreases to 1350 cm^{−1}, which is close to the experimental value of 1400 cm^{−1}. This is clear evidence of the effect of the coordination of the –COO[−] group to the TiO₂ electrode via the 2π* orbitals of COO.

We estimated the YD2–TiO₂ intermolecular interaction energy for the proposed model with and without counterpoise correction (CP) for the basis-set superposition error (BSSE), and the results are shown in Table 3. The model produces a coordinated bond at all levels of theory. When the results obtained using DFT and DFT-D3 with CP are compared, it is clear that the interaction energy is stabilized between 8.0 and 5.0 kcal mol^{−1}. The interaction energies without CP are strongly overestimated at all levels of theory. When the solvent effect is introduced, the interaction energy decreases slightly with CP. However, the interaction energy is not overestimated with both CP and the solvent effect included. There are clearly error compensation effects at this level. The magnitudes reported here are in the same range as those of similar systems, such as TPP–Zn(II)–TiO₂, which are between 56.0 and 47.0 kcal mol^{−1} [43].

On the other hand, we also performed natural population analysis (NPA) at the B3LYP-D3 level with the YD2, TiO₂,

and YD2–TiO₂ models in the gas and solvent phases. The results are summarized in Table 4 for some atoms. In general, we can see a charge transfer of 0.38e and 0.39e in the gas and solvent phases, respectively, from the YD2 to the surface of TiO₂. This can be deduced from the values in Table 4, which show that the charge on the oxygen atoms in YD2 decreases when the molecule is anchored to the TiO₂, so the charge on the Ti atoms in TiO₂ increases when the YD2 is adsorbed. In addition, the carbon atom in the anchor group becomes more positive, while the charge on the Zn atom in the porphyrin does not change significantly.

Time-dependent (TD) DFT calculations for YD2 and YD2–TiO₂

We used a range of functionals such as B3LYP, PBE, and TPSS with and without dispersion correction (D3). We finally adopted B3LYP to explore the electronic absorption process because it was the only functional that was able to correctly describe the process of charge injection from the dye to TiO₂, as shown in Fig. 3.

TDDFT has proven to be an important tool for studying the optical properties of YD2 in DSSCs. The electronic coupling in YD2–TiO₂ determines the electron injection rate and thus the conversion index (η), which involves properties that are directly related to the excited states. Thus, it is necessary to determine the properties of the excited states of YD2 and YD2–TiO₂. For porphyrins, the UV–vis absorption spectrum in the visible region usually shows a Q band, a weak T band, and a B (or Soret) band at higher energy. The calculated absorption excitation energies for YD2 and YD2–TiO₂ are reported in Table 5. The studied systems showed Q and T bands in the region between 900 nm and 500 nm and a B band at around 400 nm. When using the PBE-D3 method, as well as other reported methods such as PBEo [59], the Q band is overestimated for both YD2 and YD2–TiO₂. The data indicate that the most accurate functional for the B and Q bands is B3LYP-D3, based on a comparison of the results obtained with this functional to the corresponding experimental UV–

Table 3 Intermolecular interaction energies, E_{int} (kcal mol^{−1}), between TiO₂ ([Ti₆O₂₁H₁₈]) and YD2 with and without counterpoise correction (CP)

Method	$\Delta E_{\text{int}}^{\text{a}}$	$\Delta E_{\text{int}}^{\text{b}}$
B3LYP	−43.8	−58.9
TPSS	−41.8	−54.8
PBE	−40.2	−53.8
B3LYP-D3	−52.2	−67.4
TPSS-D3	−48.9	−61.6
PBE-D3	−45.7	−59.3
B3LYP (solv)	−40.2	−41.2
TPSS (solv)	−41.2	−41.5
PBE (solv)	−39.7	−39.6
B3LYP-D3 (solv)	−49.6	−48.6
TPSS-D3 (solv)	−48.5	−48.8
PBE-D3 (solv)	−45.1	−44.9

^a With CP

^b Without CP

Table 4 Natural population analysis (NPA) of charges on the atoms in the –CO₂[−] group of YD2 when it is free or attached to TiO₂, with both systems in either the gas or solvent phase and all results obtained at the B3LYP-D3 level of theory

System	Phase	Zn	C5	O1	O2	Ti1	Ti2
YD2–TiO ₂	Gas	1.593	0.834	−0.694	−0.647	1.470	1.551
	Solvent	1.595	0.890	−0.733	−0.713	1.495	1.573
YD2	Gas	1.592	0.734	−0.763	−0.728		
	Solvent	1.595	0.815	−0.852	−0.800		
TiO ₂	Gas					1.544	1.605
	Solvent					1.662	1.587

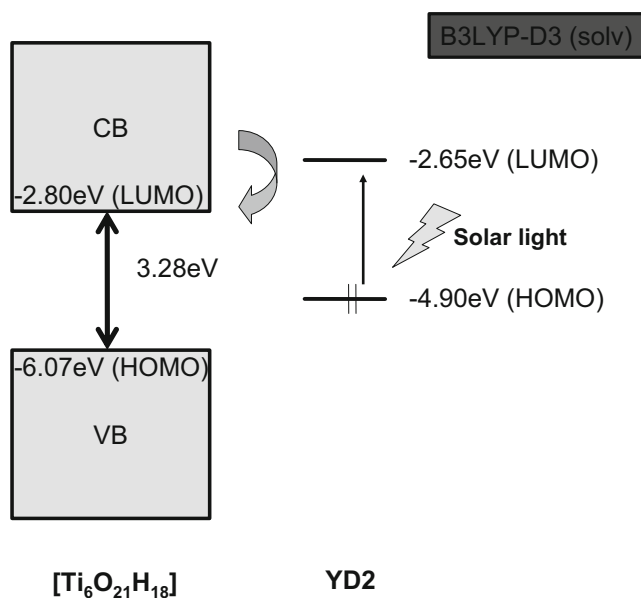


Fig. 3 Schematic energy level diagram of the absorption of solar light by YD2 and electron injection into the TiO_2 cluster

vis absorption spectrum. Thus, the B3LYP-D3 functional was used to describe the excited states of the YD2 and YD2– TiO_2 models, as discussed below.

We considered allowed transitions to be those with oscillator strengths that differ from zero. The allowed transitions obtained at the B3LYP-D3 level are shown in Figs. 4 and 5 for YD2 and YD2– TiO_2 in the solvent phase, respectively.

Table 5 Principal electronic transitions in YD2 and YD2– TiO_2 . Values shown are the B-, Q-, and T-band maxima (λ_{max}) in nm

Method	B	Q	T
YD2 (B3LYP-D3)	404	658	536
YD2 (B3LYP-D3 (solv))	438	655	516
YD2 (PBE-D3)	460	894	
YD2(PBE-D3 (solv))	470	955	
YD2 (PBEo [59])	481	902	
YD2 (CAM-B3LYP [59])	397	585	
YD2 (HSE06 [59])	423	677	
YD2 (LC- ω PBE [59])	399	628	
YD2– TiO_2 (B3LYP-D3) ^a	446	603	509
YD2– TiO_2 (B3LYP-D3 (solv)) ^a	416	656	547
YD2– TiO_2 (PBE-D3) ^a	421	743	650
YD2– TiO_2 (PBE-D3 (solv)) ^a	433	755	652
YD2 exp ^b [21]	443	646	586
YD2 exp ^c [28]	440	645	586
YD2– TiO_2 exp ^b [28]	465	650	592

^a $[\text{Ti}_6\text{O}_{21}\text{H}_{18}]$ cluster of TiO_2

^b Acetonitrile

^c Ethanol

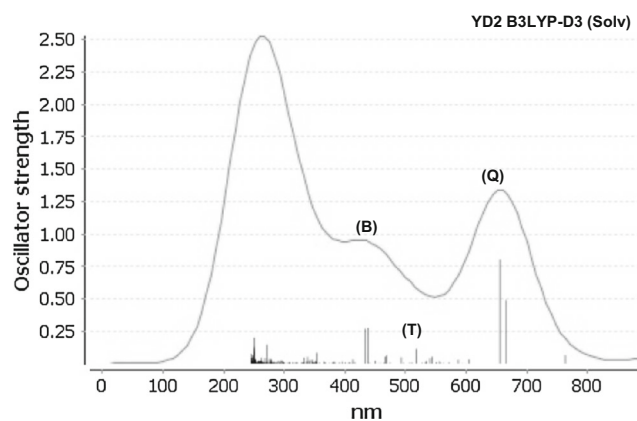


Fig. 4 Calculated B3LYP-D3 electronic spectrum of YD2 in solvent

The active molecular orbitals in the electronic transitions are shown in Figs. 6 and 7 for YD2 and YD2– TiO_2 , respectively.

YD2 The electronic structure of the YD2 model can be explored through the three absorption peaks mentioned above. The electronic transitions were assigned to individual states as ligand-to-ligand, metal-ligand-to-ligand, and metal-metal-to-ligand charge transfer (LLCT, MLLCT, and MMLCT), respectively. The results of theoretical calculations are provided in Table 6, and show good agreement with the corresponding experimental results [21, 28]. The bands represent a mixture of excitations. Band Q derives from two transitions: the transition at 666 nm consists mainly of $233a \rightarrow 236a$ ($\pi^* \rightarrow \pi^*$) and $233a \rightarrow 237a$ ($d_{zx}/d_{zy} + \pi^* \rightarrow \pi^*$). This band corresponds to LLCT and MLLCT. The second transition at 655 nm is principally linked with the excitation $233a \rightarrow 237a$ ($\pi^* \rightarrow \pi^*$), which is associated with LLCT. The frontier MOs are shown in Fig. 6. $233a$ (HOMO-2) has porphyrin π^* character, while the arrival orbitals $236a$ (LUMO) and $237a$ (LUMO+1) are mainly centered on the porphyrin and phenylethynyl carboxylic acid (LUMO); both orbitals have π^* character, and the Zn atom makes a small contribution.

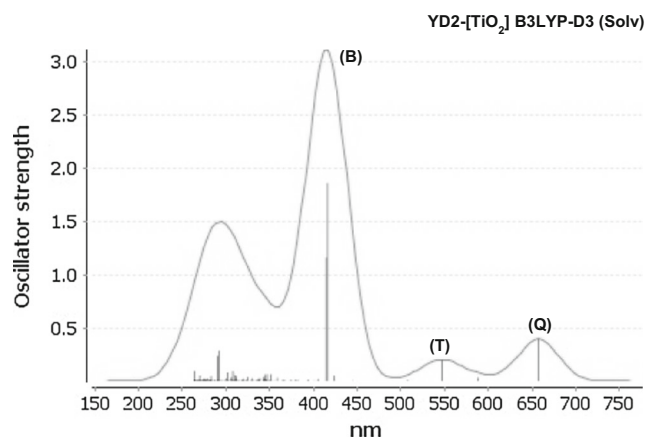
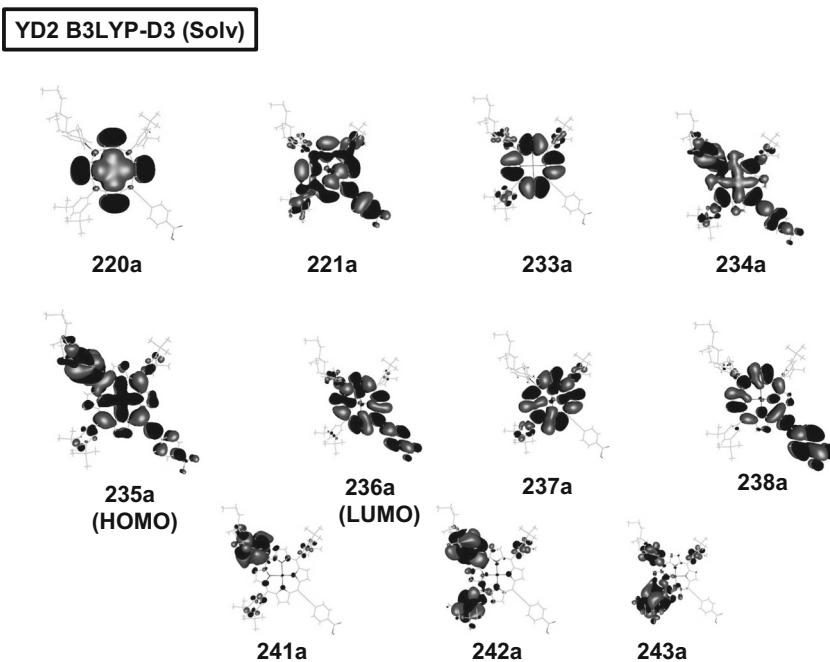


Fig. 5 Calculated B3LYP-D3 electronic spectrum of YD2– TiO_2 in solvent

Fig. 6 Most important molecular orbitals that are active in the electronic transitions of the YD2 model, as calculated at the B3LYP-D3 level in solvent



The T band is formed by a transition at 516 nm, and the principal component is 233a→238a ($\pi^* \rightarrow \pi^*$), of LLCT type. We should point out that the 233a orbital corresponds to a π^* orbital of the porphyrin ring. Thus, in this transition, charge is passed to the 238a orbital, which is mainly centered on the porphyrin and phenylethynyl carboxylic acid. Finally, the B band comprises two transitions. The one at 438 nm is mainly due to 235a→243a ($d_{zx}/d_{zy} + \pi^* \rightarrow \pi^*$), of MLLCT type. 235a

(HOMO) is a mixture of the MOs of Zn, the diarylamino group, and a small contribution from the phenylethynyl carboxylic acid, while the MO 238a (LUMO+2) contains principal contributions from the phenylethynyl carboxylic acid along with the porphyrin. The second transition at 433 nm has a principal 220a→237a ($d_{x^2-y^2} + \pi^* \rightarrow \pi^*$) excitation which is associated with MLLCT. These results are very similar to those obtained by Zhang et al. at the HSE06 level [59].

Fig. 7 Most important molecular orbitals that are active in the electronic transitions of the YD2–TiO₂ model, as calculated at the B3LYP-D3 level in solvent

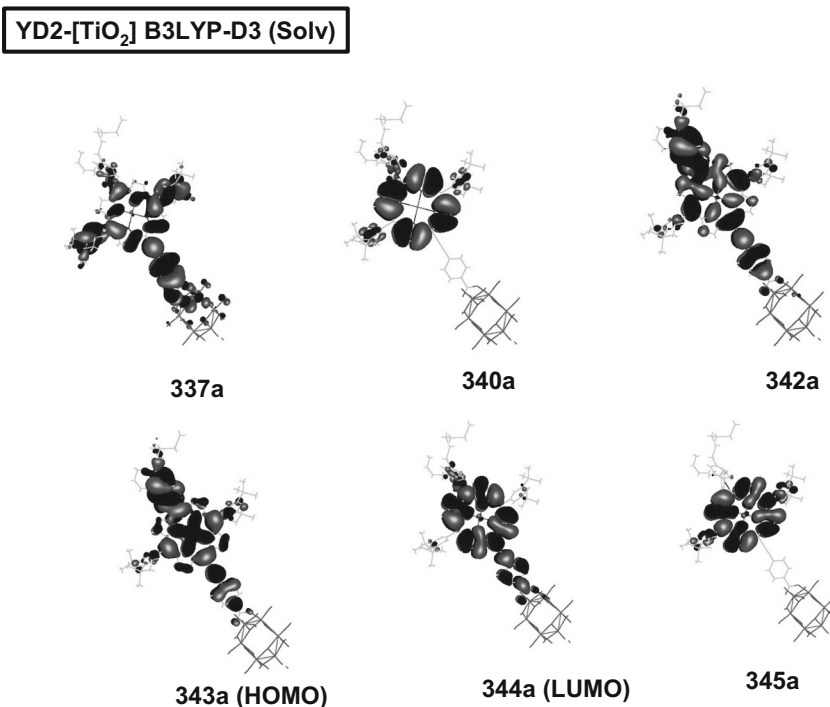


Table 6 TD-DFT/B3LYP-D3 singlet-excitation calculations for YD2 and YD2–TiO₂ in solvent

System	λ_{calc}	λ_{exp}	f^a	Contribution ^b	Transition type
YD2	666 (Q)	646	0.491	233a→236a (49 %)	LLCT ($\pi^* \rightarrow \pi^*$)
				234a→237a (39 %)	MLLCT ($d_{zx}/d_{zy} + \pi^* \rightarrow \pi^*$)
	655 (Q)		0.804	233a→237a (65 %)	MMLCT ($\pi^* \rightarrow \pi^*$)
				234a→238a (12 %)	MLLCT ($d_{zx}/d_{zy} + \pi^* \rightarrow \pi^*$)
	516 (T)	586	0.113	233a→238a (80 %)	LLCT ($\pi^* \rightarrow \pi^*$)
	438 (B)		0.274	235a→243a (45 %)	MLLCT ($d_{zx}/d_{zy} + \pi^* \rightarrow \pi^*$)
				235a→242a (35 %)	MLLCT ($d_{zx}/d_{zy} + \pi^* \rightarrow \pi^*$)
	433 (B)		0.269	220a→237a (64 %)	MLLCT ($d_{xz}/d_{yz} + \pi^* \rightarrow \pi^*$)
				221a→237a (24 %)	LLCT ($\pi^* \rightarrow \pi^*$)
				343a→344a (89 %)	MLLCT ($d_{zx}/d_{zy} + \pi^* \rightarrow \pi^*$)
YD2–TiO ₂	547 (T)	592	0.194	342a→344a (82 %)	LLLCT ($\pi^* \rightarrow \pi^*$)
	416 (B)	465	1.859	340a→345a (59 %)	LLCT ($\pi^* \rightarrow \pi^*$)
				337a→344a (9 %)	MLLCT ($\pi^* + p_z \rightarrow \pi^*$)
	414 (B)		1.163	340a→344a (50 %)	LLCT ($\pi^* \rightarrow \pi^*$)
				342a→345a (28 %)	LLCT ($\pi^* \rightarrow \pi^*$)

^a Oscillator strength^b Values are |coeff.|² × 100

YD2–TiO₂ When we used the YD2–TiO₂ model, we found a shift in the excitation bands compared with those of free YD2 (see Table 6). There was good agreement with the experimental results and the changes to the spectrum observed once YD2 was attached to TiO₂. The principal bands exhibited by free YD2 were also seen when it was bound to TiO₂. The Q band (656 nm) derives from a transition between the HOMO and LUMO of YD2: 343a→344a ($d_{zx}/d_{zy} + \pi^* \rightarrow \pi^*$), associated with MLLCT. 243a (HOMO) has contributions from porphyrin π^* , Zn, diarylamino, and phenylethynyl carboxylic acid orbitals, while 244a (LUMO) is mainly centered on the porphyrin and the phenylethynyl carboxylic acid. The Zn atom makes a small contribution to both orbitals. The frontier MOs are shown in Fig. 7.

The T band (547 nm) involves a 342a→344a ($\pi^* \rightarrow \pi^*$) transition of LLLCT type. It should be noted that the 242a (HOMO-1) orbital corresponds to a π^* orbital of the porphyrin ring and phenylethynyl carboxylic acid. Finally, the B band is associated with two transitions: that at 416 nm mainly relates to a 340a→345a ($\pi^* \rightarrow \pi^*$) transition of LLCT type. Both of these orbitals include a π^* orbital of the porphyrin ring. The second transition at 414 nm has a principal 340a→344a ($\pi^* \rightarrow \pi^*$) excitation associated with LLCT.

Absorption properties

As described in some previous papers [46, 47, 59], various fundamental variables related to experimental parameters such as the open-circuit voltage (V_{oc}) and the short-circuit current density (J_{sc}) were considered in the theoretical calculations [60]. The photoinduced electron injection that occurs in DSSCs can be viewed as a charge-transfer (CT) process.

Using the Marcus theory for electron transfer [61], the CT can be associated with the free-energy change for electron injection (ΔG^{inject}) [62]. ΔG^{inject} influences the electron injection rate and therefore the J_{sc} and V_{oc} values of the DSSC. In general, the greater the ΔG^{inject} , the greater the electron-injection efficiency (Φ^{inject}), and $\Delta G^{\text{inject}} = E^{\text{dye}^*} - E_{\text{CB}}$ [63]. E_{CB} is the reduction potential of the conduction band of TiO₂, which has an experimental (and widely used) value of -4.00 eV [64]. E^{dye^*} is the excited-state oxidation potential of the dye, which is determined by the redox potential of the

Table 7 The calculated excited-state oxidized potentials (E^{dye^*} , in eV) and free-energy changes for electron injection (ΔG^{inject} , in eV) of the Q, T, and B absorption bands for YD2 in the gas and solvent phases, as calculated at the B3LYP-D3 level. The experimentally derived value of E_{CB} (-4.00 eV) was used; the values in parentheses are ΔG^{inject} values calculated by taking E_{CB} to be the energy of the LUMO of the TiO₂ cluster

Phase	E^{dye^*}			ΔG^{inject}		
	Q	T	B	Q	T	B
Gas ^a	3.16	3.01	2.38	-0.84	-0.99	-1.62
				(+0.37)	(+0.22)	(+0.49)
Solvent ^a	3.79	3.51	2.22	-0.21	-0.49	-1.78
				(+0.78)	(+0.49)	(-0.79)
Gas ^b	3.01	2.58	1.83	-0.99	-1.42	-2.17
				(+0.22)	(-0.21)	(-0.96)
Solvent ^b	3.16	2.62	2.83	-0.84	-1.38	-1.17
				(+0.15)	(-0.39)	(-0.18)

^a E^{dye^*} is the energy of the orbital that generates the transition in the band^b E^{dye^*} is the absolute value of the HOMO energy

ground state of the dye (E^{dye}) and the vertical transition energy (λ_{max}): $E^{\text{dye}*} = E^{\text{dye}} - \lambda_{\text{max}}$. E^{dye} can be approximated to two levels: first, by applying Koopman's theorem using the absolute value of the HOMO energy [65]; second, using the energy of the orbital that generates the transition associated with the band. The calculated $E^{\text{dye}*}$ and ΔG^{inject} values for the Q, T, and B bands for DY2 in the gas and solvent phases are listed in Table 7.

The calculated $E^{\text{dye}*}$ values for the Q, T, and B bands in the gas phase are smaller than those in solvent due to a smaller ground-state oxidized potential, regardless of how E^{dye} is calculated. There is a clear effect of the solvent medium on these results. The values obtained are similar to those obtained by Zhang et al. using the HSE06 functional for YD2 [59]. On the other hand, when the experimental value of E_{CB} (−4.0 eV) was used, the values of ΔG^{inject} for YD2 were negative, meaning that the excited state of YD2 with effective charge-transfer excitation character lies above the edge of the conduction band of TiO_2 . The large absolute value of the free energy for electron injection is favorable for fast electron injection and directly proportional to the experimental values of J_{SC} and V_{OC} . However, if the theoretical value of E_{CB} is taken to be the energy of the LUMO of the TiO_2 cluster, only some values of ΔG^{inject} are negative. This shows that the proposed cluster model is only an approximation, so it is necessary to build larger systems.

Conclusions

The present investigation of the electronic structures and spectroscopic properties of the dye YD2 when it is free and when it has been adsorbed on a TiO_2 cluster provide further support for the idea that a DSSC is a supramolecular structure that is strengthened by the anchorage of the ligand on the electrode. The following points summarize the technical details required to describe these supramolecular effects:

- (1) The calculated geometric parameters are very similar, regardless of the method used to calculate them or whether the system was considered to be in the gas or solvent phase.
- (2) The coordination energy between the $-\text{COO}^-$ anchor group and TiO_2 lies between 45 and 50 kcal mol $^{-1}$ depending on the level of theory applied, showing the importance of incorporating dispersion effects.
- (3) Charge-transfer analysis shows that YD2 injects electrons into the TiO_2 cluster.
- (4) B3LYP-D3 TDDFT is the most suitable functional for describing the Q, T, and B bands of porphyrins such as those in the free YD2 and YD2– TiO_2 models. The absorption energy is centered on YD2. The LUMO of

the dye is delocalized in the region of the conduction band of the TiO_2 cluster.

- (5) MO analysis indicates that the diarylamino groups are important ligands in relation to electronic charge, and act as electron donors in the photon-induced electron injection that occurs in DSSCs.
- (6) Using the Marcus theory for electron transfer, the CT can be associated with the free-energy change for electron injection (ΔG^{inject}); both the YD2 and YD2– TiO_2 models present large absolute values of this parameter.

Acknowledgments Financial support of this work under Conicyt-Aka-ERN-001 and Fondecyt 1140503, 1140503, and 1150327 as well as Millennium Nucleus RC120001 is gratefully appreciated. N.I. wishes to acknowledge Fondecyt grant no. 11140770. C.L-F. acknowledges post-doctoral Fondecyt grant no. 3150438.

References

1. Lehn J-M, Atwood JL, Davies JED, MacNicol DD, Vögtle G (eds)(1996) Comprehensive supramolecular chemistry. Pergamon, Oxford
2. Desiraju GR (2010) J Chem Sci 122:667–675
3. Mati IK, Cockroft SL (2010) Chem Soc Rev 39:4195–4205
4. Oshovsky G, Reinhoudt D, Verboom W (2007) Angew Chem Int Ed 46:2366–2393
5. Kinge S, Crego-Calama M, Reinhoudt DN (2008) ChemPhysChem 9:20–42
6. Otero R, Gallego J, Vázquez-de-Parda A, Marín N, Miranda R (2011) Adv Mater 23:5148–5176
7. Bonifazi D, Mohnani S, Llanes-Pallas A (2009) Chem Eur J 15: 7004–7025
8. O'Regan B, Grätzel M (1991) Nature 353:737–740
9. Grätzel M (2009) Acc Chem Res 42:1788–1798
10. Gallagher KS (2013) Daedalus 142:59–77
11. Singh GK (2013) Energy 53:1–350
12. Hagfeldt A, Boschloo G, Sun L, Kloo L, Pettersson H (2010) Chem Rev 110:6595–6663
13. Imahori H, Umeyama T, Ito S (2009) Acc Chem Res 42:1809–1818
14. Pastore M, Mosconi E, De Angelis F, Grätzel M (2010) J Phys Chem C 114:7205–7212
15. De Angelis F, Fantacci S, Mosconi E, Nazeeruddin MK, Grätzel M (2011) J Phys Chem C 115:8825–8831
16. Gajardo F, Barrera M, Vargas R, Crivelli I, Loeb B (2011) Inorg Chem 50:5910–5924
17. Gajardo F, Leiva A, Loeb B, Delgadillo A, Stromberg J, Meyer G (2008) Inorg J Chim Acta 361:613–619
18. Pastore M, Fantacci S, De Angelis F (2013) J Phys Chem C 117: 3685–3700
19. Casanova D, Rotzinger FP, Grätzel M (2010) J Chem Theory Comput 6:1219–1227
20. Warnan J, Pellegrin Y, Blart E, Odobel F (2012) Chem Commun 48:675–677
21. Yella A, Lee HW, Tse H, Yi CY, Chandirian AK, Nazeeruddin MK, Diau EWG, Yeh CY, Zakeeruddin SM, Grätzel M (2011) Science 334:629–634
22. Chang Y, Wang C, Pan Y-T, Kuo H, Lo C, Hsu H, Lin C, Diau EWG (2011) Chem Commun 47:8910–8912
23. Subbaiyan NK, Hill JP, Ariga K, Fukuzumi S, D'Souza F (2011) Chem Commun 47:6003–6005

24. Bessho T, Zakeeruddin SM, Yeh C-Y, Diau EW-G, Grätzel M (2010) *Angew Chem Int Ed* 49:6646–6649
25. Silvestri F, López I, Seitz W, Martínez M, Marks TJ, Guldi D, Torres T (2009) *Chem Commun* 45:4500–4504
26. Lu H-P, Tsai C-Y, Yen W-N, Hsieh C, Lee C-W, Yeh C-Y, Diau E (2009) *J Chem Chem* 113:20990–20997
27. Li L-L, Eiau WW-G (2013) *Chem Soc Rev* 42:291–304
28. Kurotobi K, Toude Y, Kawamoto K, Fujimori Y, Ita S, Chabera P, Sundström V, Imahori H (2013) *Chem Eur J* 19:17075–17081
29. Liu S, Fu H, Cheng Y, Wu K, Ho S, Chi Y, Chou P (2012) *J Phys Chem C* 116:16338–16345
30. Kusama H, Sayama K (2012) *J Phys Chem C* 116:23906–23914
31. De Angelis F, Fantacci S, Selloni A, Nazeeruddin MK, Grätzel M (2010) *J Phys Chem C* 114:6054–6061
32. Jakubikova E, Snoeberger RC, Batista VS, Martin RL, Batista ER (2009) *J Phys Chem A* 113:12532–15540
33. Feng J, Jiao Y, Ma W, Nazeeruddin MK, Grätzel M, Meng S (2013) *J Phys Chem C* 117:3772–3778
34. Le Bahers T, Pauporté T, Lainé PP, Labat F, Adamo C, Ciofini I (2013) *J Phys Chem Lett* 4:1044–1050
35. Risplendi F, Cicero G, Mallia G, Harrison NH (2013) *Phys Chem Chem Phys* 15:235–243
36. Zarate X, Schott E, Gomez T, Arratía-Pérez R (2013) *J Phys Chem A* 117:430–438
37. Mosconi E, Yum J, Gómez C, Nazeeruddin M, Grätzel M, De Angelis F (2012) *J Am Chem Soc* 134:19438–19453
38. Maggio E, Martsinovich N, Troisi A (2012) *J Phys Chem C* 116:7638–7649
39. Yang L, Guo L, Chen Q, Yan H, Zeng Q, Zhang X, Pan X, Dai S (2012) *J Mol Graph Model* 38:82–90
40. Grimme S, Ehrlich S, Krieg H (2010) *J Chem Phys* 132:154104–154112
41. Hujo W, Grimme S (2011) *J Chem Theor Comput* 7:3866–3871
42. Syres K, Thomas A, Bondino F, Malvestuto M, Grätzel M (2010) *Langmuir* 26:14548–14555
43. Gomez T, Zarate X, Schott E, Arratia-Perez R (2014) *ESC Adv* 4:9639–9646
44. Omso KB, Peterson CS, Garcia-Lastra JM, Thygesen KS (2014) *Phys Chem Chem Phys* 16:16246–16254
45. Chaitanya K, Ju X-H, Heron BM (2014) *RSC Adv* 4:26621–26634
46. Chen J, Bai F-Q, Wang J, Hao L, Xie Z-F, Pan Q-J, Zhang H-X (2012) *Dyes Pigments* 94:459–468
47. Chen J, Wang J, Bai F-Q, Hao L, Pan Q-J, Zhang H-X (2013) *Dyes Pigments* 99:201–208
48. Casida M (1995) In: Chong DE (ed) *Recent advances in density functional methods*. World Scientific, Singapore, p 155
49. Casida ME, Jamorski C, Casida KC, Salahub DR (1998) *J Chem Phys* 108:4439–4449
50. Bauernschmitt R, Ahlrichs R (1996) *Chem Phys Lett* 256:454–464
51. Deglmann P, Furche F, Ahlrichs R (2002) *Chem Phys Lett* 362:511–518
52. Ahlrichs R, Bär M, Häser M, Horn H, Kölmel C (1989) *Chem Phys Lett* 162:165–169
53. Klamt A, Schüürman G (1993) *J Chem Soc Perkin Trans 2*(5):799–805
54. Andrae D, Häusserman M, Dolg H, Stoll H, Preuss H (1990) *Theor Chim Acta* 77:123–141
55. Bergner A, Dolg M, Küchle W, Stoll H, Preuss H (1993) *Mol Phys* 80:1431–1441
56. Dunning T, Hay P (1976) In: Schaefer H (ed) *Modern theoretical chemistry*, vol. 3. Plenum, New York, pp. 1–28.
57. Huzinaga S (1965) *J Chem Phys* 42:1293–1301
58. Eichkorn K, Treutler O, Öhm H, Häser M, Ahlrichs R (1995) *Chem Phys Lett* 240:283–289
59. Han L-H, Zhang C-R, Zhe JW, Jin N-Z, Shen Y-L, Wang W, Gong JJ, Chen Y-H, Liu Z-J (2013) *Int J Mol Sci* 14:20171–20188
60. Urbani M, Grätzel M, Nazeeruddin MK, Torres T (2014) *Chem Rev* 114:12330–12396
61. Marcus RA (1993) *Rev Mod Phys* 65:599–610
62. Fan W, Tan D, Deng W-Q (2012) *ChemPhysChem* 13:2051–2060
63. Preat J, Michaux C, Jacquemin D, Perpète EA (2009) *J Phys Chem C* 113:16821–16833
64. Asbury JB, Wang Y-Q, Hao E, Ghosh HN, Lian T (2001) *Res Chem Intermed* 27:393–406
65. Lee MJ, Balanay M, Kim D (2012) *Theor Chem Accounts* 131:1269–1278